2D Materials



RECEIVED 17 November 2020

REVISED 2 March 2021

ACCEPTED FOR PUBLICATION 22 April 2021

PUBLISHED 5 May 2021

LETTER

Significant perpendicular magnetic anisotropy in room-temperature layered ferromagnet of Cr-intercalated CrTe₂

Meng Huang¹, Zongwei Ma², Sheng Wang³, Si Li⁴, Miao Li², Junxiang Xiang¹, Ping Liu¹, Guojing Hu¹, Zengming Zhang⁵, Zhe Sun³, Yalin Lu¹, Zhigao Sheng², Gong Chen⁴, Yu-Lun Chueh⁻, Shengyuan A Yang³ and Bin Xiang¹, *©

- Hefei National Research Center for Physical Sciences at the Microscale, Department of Materials Science and Engineering, CAS Key Lab of Materials for Energy Conversion, University of Science and Technology of China, Hefei, Anhui 230026, People's Republic of China
- ² Anhui Key Laboratory of Condensed Matter Physics at Extreme Conditions, High Magnetic Field Laboratory, Chinese Academy of Sciences, Hefei 230031, People's Republic of China
- 3 National Synchrotron Radiation Laboratory, University of Science and Technology of China, Hefei, Anhui 230026, People's Republic
- ⁴ Key Laboratory of Low-Dimensional Quantum Structures and Quantum Control of Ministry of Education, Department of Physics and Synergetic Innovation Center for Quantum Effects and Applications, Hunan Normal University, Changsha 410081, People's Republic of China
- ⁵ The Centre for Physical Experiments, University of Science and Technology of China, Hefei, Anhui 230026, People's Republic of China
- ⁶ Physics Department, Georgetown University, Washington, DC 20057, United States of America
- Department of Materials Science and Engineering, National Tsing Hua University, Hsinchu 30013, Taiwan
- Research Laboratory for Quantum Materials, Singapore University of Technology and Design, Singapore 487372, Singapore
 - Anhui Laboratory of Advanced Photon Science and Technology, University of Science and Technology of China, Hefei 230026, People's Republic of China
 - * Author to whom any correspondence should be addressed.

E-mail: binxiang@ustc.edu.cn

Keywords: perpendicular magnetic anisotropy, room-temperature ferromagnetism, layered structure, anomalous Hall effect Supplementary material for this article is available online

Abstract

Magnetic anisotropy is an important characteristic of magnetic materials. Particularly, perpendicular magnetic anisotropy (PMA) is superior for the design of spintronic devices, with the advantages of scalability, endurance, thermal stability, and low switching current density. Although a series of two-dimensional (2D) or quasi-2D layered ferromagnets have been demonstrated, the room temperature intrinsic ferromagnets with PMA is rarely found. Here, we report PMA in a room-temperature layered ferromagnet of Cr-intercalated CrTe₂. By self-intercalation of the native Cr atoms, the in-plane anisotropy of CrTe₂ can be switched to PMA. Meanwhile, the Cr-intercalated CrTe₂ crystal can be easily exfoliated into thin flakes with thickness \sim 10 nm. Besides the robust PMA at room temperature, Cr-intercalated CrTe₂ also exhibits high saturation magnetization (208 emu cm⁻³ at 300 K), large anomalous Hall angle (2.23% at 300 K) and giant anomalous Hall factor (\sim 0.18 at 300 K). These excellent properties are highly desired for applications, and make Cr-intercalated CrTe₂ a distinguished candidate among all existing magnetic materials. Our work reveals a promising platform for spintronic devices and offers a new route for controlling the magnetic anisotropy in layered materials.

1. Introduction

Magnetic anisotropy, corresponding to the existence of preferred orientation of magnetic vectors, is an important characteristic for magnetic materials. It plays a critical role in stabilizing magnetic ordering in reduced dimensions, because according to the Mermin–Wagner theorem [1], without magnetic

anisotropy, magnetic long-range orders cannot exist in systems with spatial dimensions lower than three. This is demonstrated by the recent discovery of two-dimensional (2D) magnetic materials, such as CrI₃ [2], Cr₂Ge₂Te₆ [3], Fe₃GeTe₂ [4], and CrTe₂ [5].

The magnetic anisotropy also forms the basis for any practical applications of magnetic materials. Particularly, in micro- or nano-scale spintronic devices,



magnetic materials are typically made into thin layers, and a perpendicular magnetic anisotropy (PMA), where the magnetization is perpendicular to the layer plane, is desired from the application perspective [6, 7]. It has been demonstrated that compared to the in-plane anisotropy, PMA enjoys the advantages of scalability, endurance, thermal stability, and low switching current density [8–10].

Although many van der Waals (vdW) ferromagnets or intercalated vdW ferromagnets have been discovered, the scarcity of reported room temperature ferromagnets with PMA severely hinders the related spintronic applications. For example, Fe_{5-x}GeTe₂ $(T_{\rm C}\sim310$ K), ${\rm Cr_4Te_5}$ $(T_{\rm C}\sim318$ K), monolayer VSe_2 ($T_C > 300 \text{ K}$) and pristine $CrTe_2$ ($T_C \sim 310 \text{ K}$) are all room-temperature ferromagnets with in-plane magnetic anisotropy [5, 11–13]. On the other hand, PMA has also been found in ultrathin CrI_3 (\sim 61 K), $Fe_{1/4}TaS_2$ (~160 K), but their Curie temperatures are much lower than room temperature [2, 14]. It is noted that monolayer MnSe_x has a room temperature ferromagnetism, but it is PMA is very weak [15]. Moreover, besides the requirements of robust PMA and room temperature magnetism, an ideal candidate material for spintronic applications should also have the properties of large saturation magnetization for strong spin polarization and large anomalous Hall angle for good charge-to-spin conversion efficiencies [11]. The previous reported Cr₃Te₄ exhibits room temperature ferromagnetism ($T_{\rm C} \sim 317$ K) and PMA, however, its anomalous Hall angle is very low (about 0.008%) [16, 17]. Thus, searching for a new layered ferromagnet that satisfies these requirements is extremely needed and remains a challenge in the

In this paper, we report the realization of PMA in layered Cr-intercalated CrTe₂ (Cr-CrTe₂) synthesized by native Cr atoms filling the CrTe2 vdW gaps. We demonstrate that the room temperature ferromagnetism and the PMA are maintained when Cr-CrTe₂ is exfoliated into thin flakes with thickness less than 50 nm. The systematic characterizations reveal that Cr-CrTe₂ has a high Curie temperature ~310 K and a large saturation magnetization of 211 emu cm⁻³ at 300 K, satisfying the requirements for an ideal spintronic material. The band structure characterized by angle-resolved photoemission spectroscopy (ARPES) reveals a semi-metallic behavior in Cr-CrTe2. Moreover, we investigate the anomalous Hall transport and uncover an extremely large anomalous Hall factor (\sim 0.23 at 200 K and 0.18 at 300 K) which exceeds other popular magnetic materials. Our work holds great promise for layered magnet based spintronic applications.

2. Results and discussion

The Cr-CrTe₂ crystal samples are synthesized by an indirect approach through the oxidation of

 $K_x Cr_{1.3} Te_2$ (0 < x < 0.7) with iodine in acetonitrile (see section 4 for the detailed approach) [18]. The image of as-synthesized Cr-CrTe2 crystals is shown in the inset of figure 1(b), demonstrating a plate-like shape with metallic luster. The inductively coupled plasma-atomic emission spectrometer was utilized to quantify the chemical contents of the Cr-CrTe2 samples (table S2(available online at stacks.iop.org/ 2DM/8/031003/mmedia), supplementary information), revealing a mole ratio of Cr:Te = 1.33:2.00. By tuning the molar ratio in the precursor, we have also successfully synthesized the CrTe2 crystals for a comparative study (note S1, supplementary information). Figure 1(a) shows the crystal structure of CrTe₂ and Cr-CrTe₂. CrTe₂ is a vdW layered material with space group $P\bar{3}$ m1. The determined lattice parameters obtained from refinement were a = b = 3.7830 Åand c = 6.0958 Å (figure S1, supplementary information), which is very close to the values in previous report [18]. Figure 1(b) shows the x-ray diffraction (XRD) pattern of Cr-CrTe2 single-crystal. Only (00L) peaks are observed, suggesting the crystal surface is normal to the c axis. Figure 1(c) shows the experimental and the Rietveld refinement profiles of the powder XRD pattern for Cr-CrTe₂ sample. The experimental XRD pattern can well fitted with $P\bar{3}m1$ group. The refinement shows that Cr-CrTe2 crystal maintains the layered structure of the host CrTe2 and contains two Cr (Cr 1, Cr 2) and one Te sites, as shown in figure 1(a). Excess Cr atoms (Cr 2) occupy the octahedral vacancies of Te atoms in the vdW gap of CrTe₂ with fractional sites occupations. The occupancy rate of Cr 2 sites is \sim 30%. The lattice parameters were a = b = 3.7908 Å and c = 6.1144 Å. The expansion of cell parameters in Cr-CrTe2 further confirmed the excess Cr atoms intercalate into the layer of CrTe2, which is consistent with previous work [19]. Meanwhile, it exhibits distinct crystal structure from the reported Cr_2Te_3 [20], Cr_3Te_4 [16, 17] and Cr_5Te_8 [21] (figure S2, supplementary information). To further confirm the crystal structure of Cr-CrTe₂, we conduct electron beam diffraction characterizations along different crystal zone axis of [001] and [111] in transmission electron microscopy (TEM). The obtained electron diffraction patterns are consistent with our simulated results (figure S3, supplementary information). The high-resolution TEM image of the as-grown Cr-CrTe2 crystal reveals a 0.35 nm distance between the adjacent (100) planes (figure S4, supplementary information).

Next, we characterize the magnetic properties. 1T-CrTe₂ shows a ferromagnet with a Curie temperature \sim 316 K (figure S5, supplementary information), which is consistent with previous report [5]. Figures 2(a) and (b) show the temperature dependence of magnetization M(T) under H=0.1 T and 1 T applied along c axis and ab plane, respectively. As shown in the inset of figure 2(a), Curie temperature of Cr-CrTe₂ is \sim 312 K, which is roughly

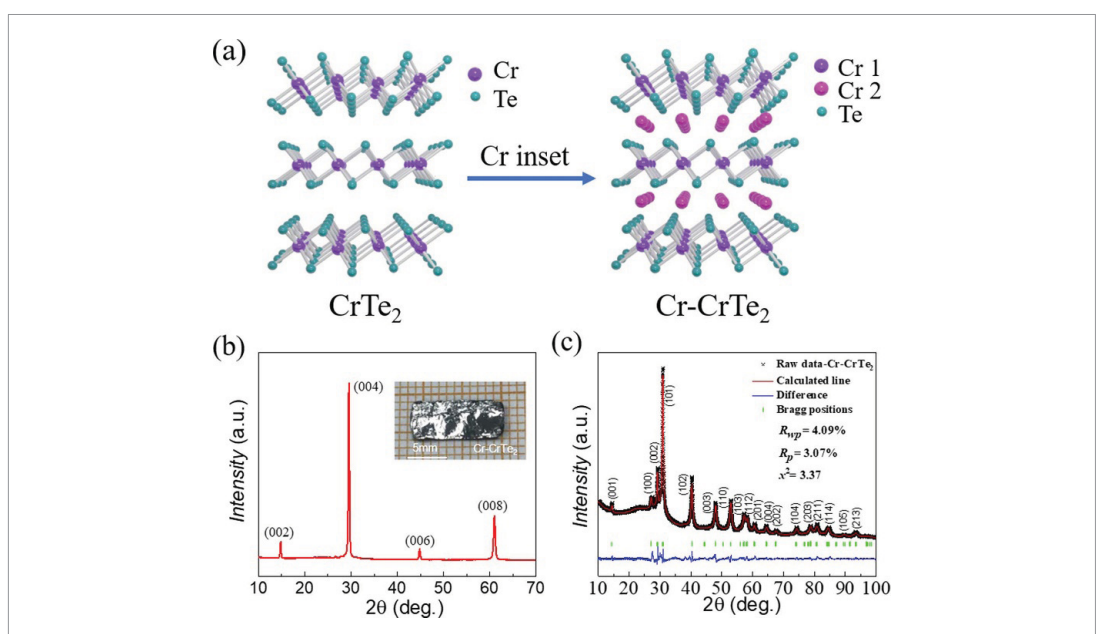


Figure 1. Characterization of as-grown Cr-intercalated CrTe₂ crystal. (a) Crystal structure of CrTe₂ and Cr-CrTe₂. (b) X-ray diffraction pattern of a Cr-CrTe₂ single crystal measured on the (00l) surface. (c) Rietveld refined powder XRD pattern at room temperature for the Cr-CrTe₂ crystal. The vertical marks (green bars) highlight the positions of the allowed Bragg reflections, while the solid line (blue line) highlight the differences between the acquired and calculated patterns.

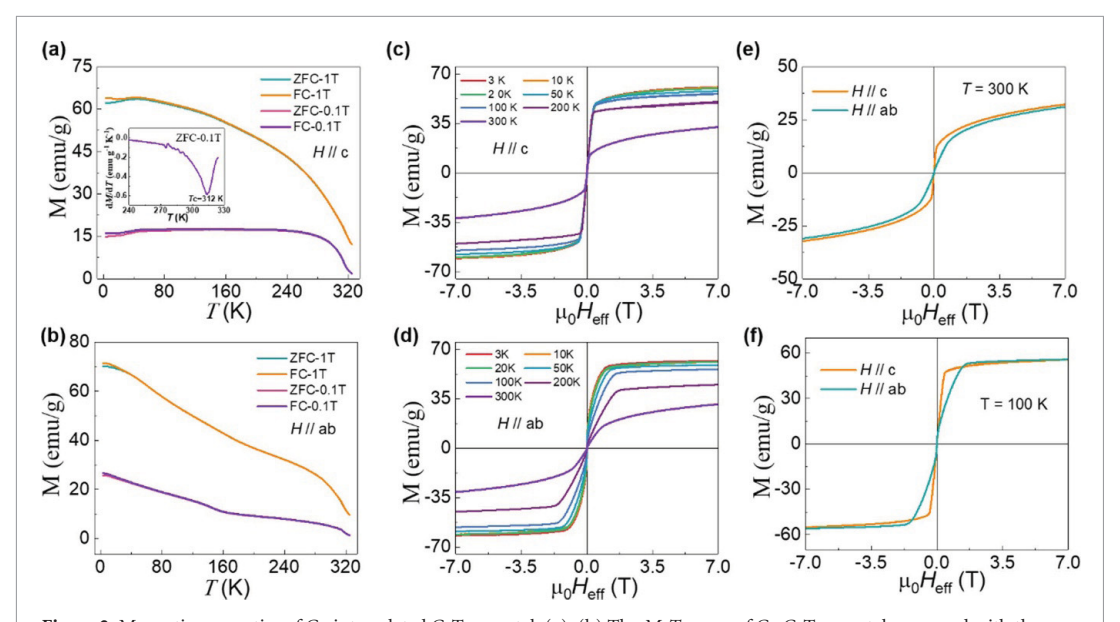


Figure 2. Magnetic properties of Cr-intercalated CrTe₂ crystal. (a), (b) The M-T curve of Cr-CrTe₂ crystal measured with the external magnetic field H = 0.1 T and 1 T applied along the c axis and in the ab plane under ZFC and FC mode. The inset of figure (a) is the dM/dT vs T of the ZFC curves for H = 0.1 T. (c), (d) Field dependence of magnetization (M) at indicated temperatures with H//c axis and H//ab plane. (e), (f) M-H curves at 300 K and 100 K, showing a perpendicular magnetic anisotropy.

determined from the minima of the dM/dT curves under H=0.1 T with ZFC mode. For 1T-CrTe₂, the M-H curves (figure S6, supplementary information) show that the in-plane magnetization is saturated while the out-of-plane magnetization is still unsaturated, when the external magnetic field reaches \sim 7 T. This shows that CrTe₂ has an in-plane magnetic anisotropy, which is consistent with previous works [5]. Figures 2(c) and (d) show effective magnetic

field $\mu_0 H_{\rm eff}$ dependence of magnetization at indicated temperatures with H//c axis and H//ab plane for Cr-CrTe₂ crystal, respectively. Here, the effective magnetic field $\mu_0 H_{\rm eff} = \mu_0~(H-N_{\rm d}M)$, where $N_{\rm d}$ is the demagnetization factor and M is the measured magnetization. For a crystal of Cr-CrTe₂ with dimensions $3.52 \times 3.35 \times 0.27$ mm, the calculated value of $N_{\rm d}$ is 0.84 [22]. However, a distinct behavior is observed in Cr-CrTe₂ at 300 K and 100 K, where the



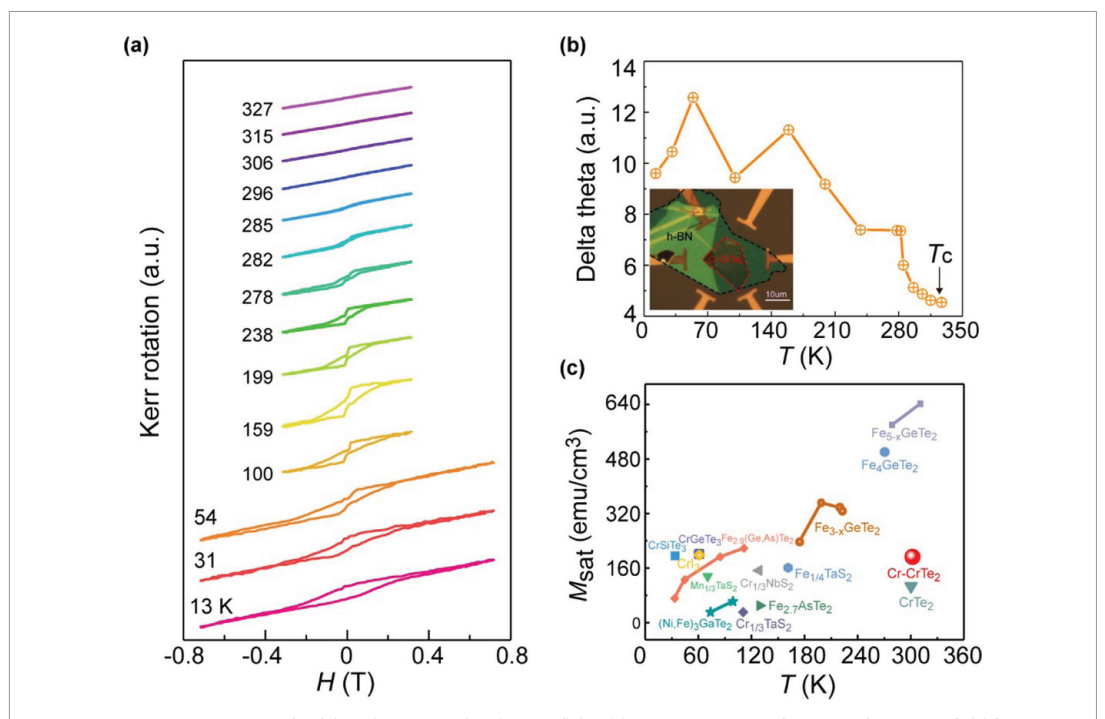


Figure 3. Magnetic properties of exfoliated Cr-intercalated CrTe₂ flake. (a) Kerr rotation as a function of magnetic field for exfoliated Cr-CrTe₂ flake at various temperature with magnetic field applied along c axis. (b) The plot of delta Kerr rotation as a function of temperature, indicating a Curie temperature of 306 K, consistent with our M-T curve result ($T_c = 309$ K). The delta Kerr rotation is calculated using Kerr rotation at H = 315 mT minus Kerr rotation at H = -315 mT. (c) Saturation magnetization and Curie temperature of Cr-CrTe₂ compared to other 2D and quasi-2D ferromagnets [5, 11, 14, 23–31].

out-of-plane/in-plane M-H loops in Cr-CrTe $_2$ crystal exhibit easy-/hard-axes behavior (figures 2(e) and (f)). This demonstrates the realization of PMA in Cr-CrTe $_2$, which is different from CrTe $_2$. We estimated the effective magnetic anisotropy $K_{\rm eff}$ of Cr-CrTe $_2$ (note S6, supplementary information). The calculated $K_{\rm eff}$ at 300 K and 100 K have values of 7.55×10^4 J m $^{-3} > 0$ and $1.08 \times 10^5 > 0$, further confirming the PMA in Cr-CrTe $_2$. At low temperature (T < 10 K), the Cr-CrTe $_2$ exhibits weak in-plane magnetic anisotropy, confirmed by the calculated effective magnetic anisotropy of $K_{\rm eff} < 0$ (table S5, supplementary information).

Our characterization has been done for a range of different samples with different thicknesses, and the results are consistent. Similar to $CrTe_2$, we find that thin flakes of $Cr-CrTe_2$ can also be readily exfoliated from the bulk sample. In our experiment, the thinnest sample that we characterized has a thickness of ~ 10 nm (figure S7, supplementary information). In the following discussion, we will mostly focus on the results from a thin flake sample with thickness about 45 nm.

The result of polar magneto-optical Kerr effect (MOKE) characterization on this thin flake sample is shown in figures 3(a) and (b), plotted as a function of the external magnetic field perpendicular to the thin flake surface at different temperatures. In order to determine the Curie temperature more clearly, we also plot the Kerr rotation versus applied magnetic

field near $T_{\rm C}$ (figure S8, supplementary information). We can observe a clear nonlinear sign at 306 K, showing that the Curie temperature of this Cr-CrTe₂ flake (45 nm) still has a value above $T_{\rm C} > 306$ K, which is slightly lower than the $T_{\rm C}$ (312 K) of bulk Cr-CrTe₂ crystal from the M-T curve. The measurement also finds a saturation magnetization of ~ 211 emu cm⁻³ from the M-H curve at 300 K. These results demonstrate that Cr-intercalated CrTe₂ shows room temperature ferromagnetism, PMA, and high saturation magnetization (211 emu cm⁻³ at 300 K). A comparison to other layered ferromagnets is shown in figure 3(c).

We have also probed the band structure of asgrown Cr-CrTe₂ crystal by using the ARPES. The constant energy contours of Cr-CrTe2 at 350 meV binding energy acquired by ARPES and the sketch of projected 2D Brillouin zone (BZ) are illustrated in figure 4(a). One can observe a hexagonal-shaped constant energy contour centered at Γ point. Figures 4(b) and (c) show the ARPES intensities along Γ -K-M and Γ -M- Γ direction, respectively. We identify the hexagonal-shaped contour as a hole pocket from band dispersions. Notably, there are also some electronic pocket features around the boundary of the BZ and the bottom of the conduction band is located at around -100 meV with respect to the binding energy. Through fitting, we find that the top of the valence band is also very close to the Fermi level. The location of the top of valence band is 380 and

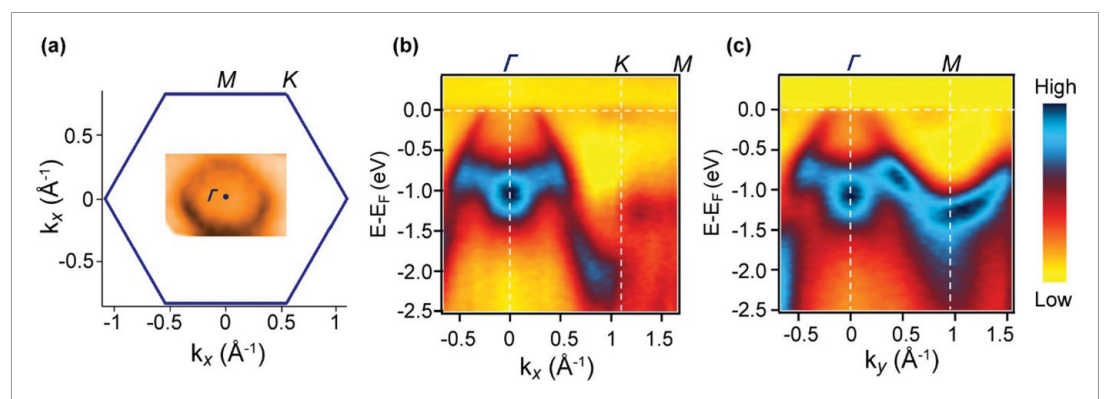


Figure 4. ARPES band mapping. (a) The sketch of projected 2D Brillouin zone, showing a hexagonal-shaped constant energy contour centered at Γ point. (b), (c) The ARPES intensity along Γ -K-M and Γ -M- Γ direction, respectively.

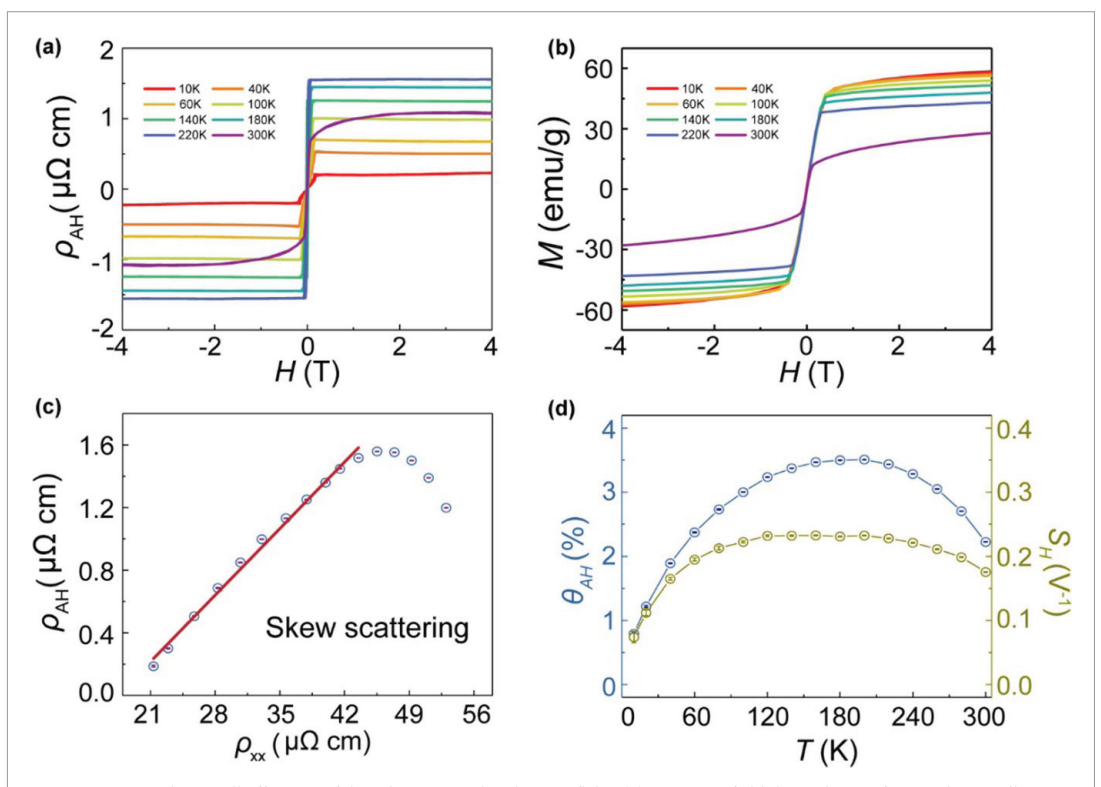


Figure 5. Anomalous Hall effect in exfoliated Cr-intercalated CrTe₂ flake. (a) Magnetic field dependence of anomalous Hall resistivity of Cr-CrTe₂ at various temperature for the current applied in the a-b plane and magnetic field applied along c axis. (b) Magnetic field dependence of magnetization for H//c at various temperature. (c) Scaling behavior of ρ_{AHE} vs ρ_{xx} with a linear scaling relation in a large resistivity range, revealing the skew scattering mechanism dominating the AHE. (d) Temperature dependence of anomalous Hall angle and anomalous Hall factor in exfoliated Cr-intercalated CrTe₂ flake.

110 meV above the Fermi level for Γ -K-M and Γ -M- Γ direction, respectively. As indicated by band calculations for related compounds [18, 32–34], there are multiple bands across the Fermi levels around the zone center. Since these bands are close to each other, the broadening of their spectral weight makes it difficult to distinguish individual dispersions clearly. The data in figure 4 were taken using different light polarizations with respect to the wavefunctions in the BZ, and the photoemission matrix element effect can modulate the spectral weight with emphasis on different bands. This effect helps us identify different

bands around the zone center. On the basis of these results we conclude that Cr-CrTe₂ is a ferromagnetic semimetal.

To further characterize the magnetism in the mechanically exfoliated Cr-intercalated CrTe₂ thin flakes, we carry out the Hall transport measurements under a perpendicular magnetic field at the temperatures varying from 3 K to 300 K. Figure 5(a) shows the extracted anomalous Hall resistivity ($\rho_{\rm AH}$) of Cr-intercalated CrTe₂ thin flake as a function of the external magnetic field measured at different temperatures. The field dependence of $\rho_{\rm AH}$ resembles

the M-H curves (figure 5(b)), which is a typical feature for ferromagnets. The hysteresis loop in ρ_{AH} is not obvious due to the small coercive field (<100 Oe) in Cr-intercalated CrTe₂. The Hall coefficient R_H is positive from 10 K to 300 K, indicating the hole-type carrier in Cr-CrTe₂, consistent with our ARPES measurement. The carrier concentration is found to be 1.02×10^{21} cm⁻³ at 10 K from the relation $n = 1/|eR_H|$, where e is the charge of an electron.

To understand the dominant mechanism of the anomalous Hall effect (AHE) in Cr-intercalated CrTe₂, we study the scaling relation between the anomalous Hall resistivity and longitudinal resistivity. Generally, there are three recognized AHE mechanisms, namely, intrinsic mechanism, extrinsic side jump and skew scattering mechanisms [35]. In simple pictures, the intrinsic mechanism and extrinsic side jump mechanism both give a quadratic relationship of $\rho_{AH} \propto \rho_{xx}^2$ between the anomalous Hall resistivity and longitudinal resistivity. On the other hand, the skew-scattering mechanism gives a linear relationship of $\rho_{AH} \propto \rho_{xx}$. Figure 5(c) exhibits a clear linear relationship between the anomalous Hall resistivity and longitudinal resistivity below 220 K, indicating that the skew scattering mechanism dominating the AHE in Cr-CrTe₂ at low temperatures. As discussed above, the Cr-CrTe2 crystal is formed from CrTe2 by filling the vdW gaps through a self-intercalation process of Cr atoms. This process could naturally introduce lattice defects in Cr-intercalated CrTe₂ samples. It is likely that the skew scattering mainly occurs at these defects associated with the intercalation [36, 37].

The AHE strength is usually characterized by two key characteristic parameters, the anomalous Hall angle θ_{AH} and anomalous Hall factor S_H . The anomalous Hall angle is defined as $\theta_{AH} = \sigma_{AH}/\sigma_{xx}$, where σ_{AH} and σ_{xx} are the anomalous Hall conductivity and the longitudinal conductivity, respectively. It measures the ratio of the normal longitudinal charge current to the anomalous Hall current. S_H is defined by $S_{\rm H} = \sigma_{\rm AH}/M$, which evaluates the ratio of the anomalous Hall current to the magnetization. We plot θ_{AH} and S_H for Cr-CrTe₂ as a function of temperature varying from 2 K to 300 K, as shown in figure 5(d). One observes that θ_{AH} increases quickly with the temperature and takes a maximum value 3.5% at 180 K. It shows a parabolic like shape in the whole temperature range. On the other hand, S_H increases slowly at low temperature region and keeps a constant above 60 K. The values of θ_{AH} and S_{H} are 2.23% and 0.18 at 300 K, respectively.

These θ_{AH} and S_H values indicate that the AHE in Cr-intercalated CrTe₂ is quite remarkable. In figure 6, we compare θ_{AH} and S_H values of Cr-intercalated CrTe₂ with other popular ferromagnets [23, 38–41]. One can see that Cr-intercalated CrTe₂ stands out in the figure. It exhibits relatively high θ_{AH} , larger than most other materials. And it has a giant S_H , which is the largest among all these ferromagnetic materials.

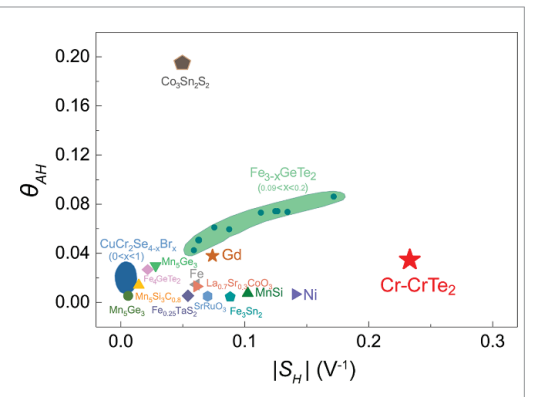


Figure 6. Anomalous Hall angle θ_{AH} versus anomalous Hall factor S_H for as-grown Cr-intercalated CrTe₂ and other popular ferromagnets. Cr-intercalated CrTe₂ exhibits relatively high θ_{AH} and giant S_H simultaneously, compared to other popular ferromagnets. The absolute value of θ_{AH} and S_H of other ferromagnets are taken from the reported references (table S7, supplementary information).

The giant $S_{\rm H}$ is mainly due to the large $\sigma_{\rm AH}$ (up to 925 $\Omega^{-1}\,{\rm cm}^{-1}$) (figure S9, supplementary information). In the figure, we see that Fe₃GeTe₂ also has a large $\theta_{\rm AH}$ of 7% and $S_{\rm H}$ of 0.17 at 10 K. However, its low $T_{\rm C}$ (~220 K) limits the possible room temperature applications. There has been attempts to boost up the $T_{\rm C}$ of Fe₃GeTe₂, e.g. by ionic liquid gating or by constructing a hetero-structure of Fe₃GeTe₂/Bi₂Te₃ through molecular-beam epitaxy [42, 43]. However, these methods are hard to implement for practical applications. In contrast, Cr-intercalated CrTe₂ hosts intrinsic ferromagnetism above 300 K, making its strong AHE readily implemented for applications.

3. Conclusion

In summary, we have synthesized a new layered magnetic material Cr-CrTe₂. We reveal that it is an ideal spintronic material, which exhibits room-temperature ferromagnetism, PMA and large magnetization. These excellent properties are maintained even when the material is thinned down to thicknesses below 50 nm. Furthermore, we find that Cr-CrTe₂ possesses a huge AHE. Particularly, its anomalous Hall factor is larger than other ferromagnets reported to date. Our work not only discovers a new material, Cr-CrTe₂, which bears the full potential to serve as a building block for spintronic devices, but also offers a new approach to control the magnetic anisotropy in layered materials.

4. Materials and methods

4.1. Synthesis of Cr-intercalated CrTe₂ crystal

The Cr-intercalated CrTe₂ single crystal was synthesized indirectly by oxidation of K_x Cr_{1.3}Te₂ (0 < x < 0.7) with iodine in acetonitrile. Firstly, Cr (99.95%, aladdin) and Te (99.99%, aladdin) powders with the molar ratio (Cr:Te = 1.3:2) were thoroughly mixed



and then loaded in quartz tube. Secondly, we added K with the molar ratio (K:Cr:Te = 1:1.3:2) in a glove box because K is sensitive to air and water. Then the quartz tube was sealed in vacuum, and heated up to 900 °C, kept under this temperature for seven days. After back to room temperature, the growth quartz tube was opened in a glove box considering $K_xCr_{1.3}Te_2$ was sensitive to air and water. Then we obtained the single crystal $K_xCr_{1.3}Te_2$ (0 < x < 0.7). Single crystal $K_xCr_{1.3}Te_2$ was then added into solutions of iodine in acetonitrile to remove the K ions through de-intercalation reaction

$$2K_xCr_{1.3}Te_2 + xI_2 = 2Cr_{1.3}Te_2 + 2x KI.$$
 (1)

A slight excess of iodine was added into the acetonitrile to ensure that K atoms in $K_xCr_{1.3}Te_2$ were removed completely. Finally, the $Cr_{1.3}Te_2$ sample was filtered, washed with acetonitrile repeatedly and dried under vacuum.

We also prepared $CrTe_2$ single crystal for comparison (note S1, supplementary information). Magnetization measurements of as-grown $Cr-CrTe_2$ and $CrTe_2$ single crystals were carried out by applying external magnetic field parallel to the *ab* plane and *c* axis using a vibrating sample magnetometer (MPMS 3, Quantum Design).

4.2. Inductively coupled plasma atomic emission spectrometry (ICP-AES) measurements

Inductively coupled plasma atomic emission spectrometry (ICP-AES, Optima 7300 DV) was used to determine the element molar ratio. To prepare a solution of ICP-AES, certain amount of Cr-CrTe₂ and CrTe₂ single crystal was dissolved in aqua regia (mixture of nitric acid and hydrochloric acid) and sonicating the mixture for about 1 h at 80 K. The solution was diluted by adding DI (Deionized Water) water to make the element concentration below 80 ppm. All the solution was tested under the same setup and parameters of the same ICP-AES.

4.3. Exfoliated flake-based device fabrication

Firstly, the standard Hall bar electrodes with Ti (8 nm)/Au (25 nm) was fabricated on a SiO $_2$ (285 nm)/Si (500 μ m) substrate using ultra-violet lithography (SUSS MBA6), followed by metal deposition and a lift-off process. Then, using an all-dry viscoelastic stamping technique inside argon gas filled glove-box, the Cr-intercalated CrTe $_2$ flakes obtained by mechanically exfoliation was transferred onto the pre-patterned Ti/Au Hall geometry through our home-made transfer station in a glove box. Hexagonal boron nitride (h-BN) was capped on the device top and utilized to prevent degradation during further characterizations. The thickness of Cr-CrTe $_2$ flakes were measured using atomic force microscope (Bruker, Demension Icon) in tapping mode.

4.4. MOKE measurements

The Cr-intercalated CrTe2 flakes were transferred onto the center of the six electrodes for positioning and encapsulated by h-BN. The MOKE was measured in a cryostat with a 434.6 mT magnet. The laser of 532 nm wavelength was polarized by a Glan prism, and focused on the sample by an 50× objective lens to form a spot of diameter D = 4um. The reflected probe beam from sample surface was sent to the Wollaston polarizer to detect the output signal voltage using two Si photo-diodes. The SR865 lock-in amplifier and 2182 nanovoltmeter were used to record the output signal. The difference of two output signal voltage divided by the sum of two output signal voltage determines the Kerr rotation angle. The magnetic field is applied perpendicular to sample surface and the laser power is 9.1 μ W to avoid local heating.

4.5. ARPES measurements

The ARPES measurements were performed at beamline 13 U of the National Synchrotron Radiation Laboratory at Hefei, China, with a Scienta Omicron DA30L analyzer. The overall energy resolution is better than 20 meV, and the angular resolution is 0.3°. Single crystal samples were cleaved in ultrahigh vacuum better than 5×10^{-10} mbar to achieve clean surfaces, and ARPES measurements were performed using s-polarized photons at sample temperature \sim 300 K.

4.6. Transport measurements

Transport measurements of exfoliated Cr-intercalated CrTe₂ were performed in physical property measurement system (Quantum Design, PPMS-9 T). The longitudinal resistivity and Hall resistivity were measured using a standard four-probe method with a constant alternating current of 1 mA flowing in the *ab* plane. For Hall resistivity, we performed the antisymmetrization procedure ($\rho_{xy}(H) = [\rho_{xy}(+H) - \rho_{xy}(-H)]/2$) to remove the longitudinal resistivity contribution, where H is the applied magnetic field, $\rho_{xy}(+H)$ is Hall resistivity sweeping from the positive field to negative field, $\rho_{xy}(-H)$ is Hall resistivity sweeping from the negative field to positive field.

Data availability statement

The data that support the findings of this study are available upon reasonable request from the authors.

Acknowledgments

This work was supported by the National Key Research and Development Program of China (2017YFA0402900), Singapore MOE AcRF Tier 2 (MOE2017-T2-2-108) and the US NSF (DMR-2005108). The research is also supported by Ministry



of Science and Technology through Grant Nos. 108-2218-E-007-045-, 107-2923-E-007-002-MY3, 107-2218-E-007-055-, 107-2112-M-007-030-MY3 and 109-2634-F-007-023. This research was partially carried out at the USTC Center for Micro and Nanoscale Research and Fabrication.

ORCID iDs

Meng Huang https://orcid.org/0000-0001-6493-8223

Zongwei Ma https://orcid.org/0000-0002-9328-9194

Ping Liu https://orcid.org/0000-0002-8985-6803 Zengming Zhang https://orcid.org/0000-0001-8245-9955

Zhigao Sheng • https://orcid.org/0000-0003-3382-5968

Yu-Lun Chueh https://orcid.org/0000-0002-0155-9987

Bin Xiang https://orcid.org/0000-0001-8254-8640

References

- [1] Mermin N D and Wagner H 1966 Phys. Rev. Lett. 17 1133-6
- [2] Huang B et al 2017 Nature 546 270-3
- [3] Gong C et al 2017 Nature **546** 265–9
- [4] Tan C, Lee J, Jung S-G, Park T, Albarakati S, Partridge J, Field M R, McCulloch D G, Wang L and Lee C 2018 Nat. Commun. 9 1554
- [5] Sun X et al 2020 Nano Res. 13 3358-63
- [6] Miron I M, Garello K, Gaudin G, Zermatten P-J, Costache M V, Auffret S, Bandiera S, Rodmacq B, Schuhl A and Gambardella P 2011 Nature 476 189–93
- [7] Han J, Richardella A, Siddiqui S A, Finley J, Samarth N and Liu L 2017 *Phys. Rev. Lett.* **119** 077702
- [8] Lim H, Lee S and Shin H 2016 Act. Passive Electron. Compon. 2016 3858621
- [9] Nishimura N, Hirai T, Koganei A, Ikeda T, Okano K, Sekiguchi Y and Osada Y 2002 J. Appl. Phys. 91 5246–9
- [10] Mangin S, Ravelosona D, Katine J, Carey M, Terris B and Fullerton E E 2006 Nat. Mater. 5 210–5
- [11] Seo J et al 2020 Sci. Adv. 6 eaay8912
- [12] Zhang L-Z et al 2020 Phys. Rev. B 101 214413
- [13] Bonilla M, Kolekar S, Ma Y, Diaz H C, Kalappattil V, Das R, Eggers T, Gutierrez H R, Phan M-H and Batzill M 2018 Nat. Nanotech. 13 289–93

- [14] Checkelsky J G, Lee M, Morosan E, Cava R J and Ong N P 2008 Phys. Rev. B 77 014433
- [15] O'Hara D J et al 2018 Nano. Lett. 18 3125-31
- [16] Dijkstra J, Weitering H, van Bruggen C, Haas C and de Groot R 1989 J. Phys. Condens. Matter 1 9141
- [17] Yamaguchi M and Hashimoto T 1972 J. Phys. Soc. Japan 32 635–8
- [18] Freitas D C, Weht R, Sulpice A, Remenyi G, Strobel P, Gay F, Marcus J and Núñez-Regueiro M 2015 J. Phys. Condens. Matter 27 176002
- [19] Morosan E, Zandbergen H W, Dennis B S, Bos J W G, Onose Y, Klimczuk T, Ramirez A P, Ong N P and Cava R J 2006 Nat. Phys. 2 544–50
- [20] Hamasaki T, Hashimoto T, Yamaguchi Y and Watanabe H 1975 Solid State Commun. 16 895–7
- [21] Wang Y H et al 2019 Phys. Rev. B 100 024434
- [22] Aharoni A 1998 J. Appl. Phys. 83 3432-4
- [23] Kim K et al 2018 Nat. Mater. 17 794
- [24] Miyadai T, Kikuchi K, Kondo H, Sakka S, Arai M and Ishikawa Y 1983 *J. Phys. Soc. Japan* **52** 1394–401
- [25] McGuire M A, Dixit H, Cooper V R and Sales B C 2015 Chem. Mater. 27 612–20
- [26] Zhang H et al 2018 Appl. Phys. Lett. 113 072402
- [27] Yamasaki Y, Moriya R, Arai M, Masubuchi S, Pyon S, Tamegai T, Ueno K and Machida T 2017 2D Mater. 4 041007
- [28] May A F, Ovchinnikov D, Zheng Q, Hermann R, Calder S, Huang B, Fei Z, Liu Y, Xu X and McGuire M A 2019 ACS Nano 13 4436–42
- [29] Chen B, Yang J, Wang H, Imai M, Ohta H, Michioka C, Yoshimura K and Fang M 2013 J. Phys. Soc. Japan 82 124711
- [30] Kuznetsov A N, Stroganova E A, Zakharova E Y, Solopchenko A V, Sobolev A V, Presniakov I A, Kirdyankin D I and Novotortsev V M 2017 J. Solid State Chem. 250 90–9
- [31] Casto L et al 2015 APL Mater. 3 041515
- [32] Yang X, Zhou X, Feng W and Yao Y 2021 Phys. Rev. B 103 024436
- [33] Li S, Wang -S-S, Tai B, Wu W, Xiang B, Sheng X-L and Yang S A 2021 *Phys. Rev.* B **103** 045114
- [34] Lv H Y, Lu W J, Shao D F, Liu Y and Sun Y P 2015 *Phys. Rev.* B **92** 214419
- [35] Nagaosa N, Sinova J, Onoda S, MacDonald A H and Ong N P 2010 Rev. Mod. Phys. 82 1539
- [36] Smit J 1955 Physica 21 877-87
- [37] Smit J 1958 Physica 24 39-51
- [38] Liu E et al 2018 Nat. Phys. 14 1125-31
- [39] Nakatsuji S, Kiyohara N and Higo T 2015 Nature 527 212-5
- [40] Wang Q, Sun S, Zhang X, Pang F and Lei H 2016 Phys. Rev. B 94 075135
- [41] Sürgers C, Fischer G, Winkel P and Löhneysen H V 2014 Phys. Rev. B 90 104421
- [42] Deng Y J et al 2018 Nature **563** 94–9
- [43] Wang H et al 2020 ACS Nano 14 10045–53